PHILOSOPHICAL TRANSACTIONS A

Phil. Trans. R. Soc. A.

doi:10.1098/not yet assigned

Multiscale Damage Modeling in a Ceramic Matrix Composite using a Finite Element Microstructure MEshfree methodology[1]

L. Saucedo Mora[1] and T.J. Marrow*[2]

1 Institute Eduardo Torroja for Construction Sciences-CSIC, Madrid, Spain
2 Department of Materials, University of Oxford, UK

Keywords: Multi-scale modelling, cellular automata, finite element, damage, composites

---

[1] Authors' copy of a paper accepted for publication. *Phil. Trans. R. Soc. A* 20150276. http://dx.doi.org/10.1098/rsta.2015.0276

PHILOSOPHICAL TRANSACTIONS A

Phil. Trans. R. Soc. A.

doi:10.1098/not yet assigned

Summary

The problem of multi-scale modelling of damage development in a SiC ceramic fibre reinforced SiC matrix ceramic composite tube is addressed, with the objective of demonstrating the ability of the FEMME (Finite Element Microstructure Meshfree) model to introduce important aspects of the microstructure into a larger scale model of the component. These are particularly the location, orientation and geometry of significant porosity and the load-carrying capability and quasi-brittle failure behaviour of the fibre tows. The FEMME model utilises finite element and cellular automata layers, connected by a meshfree layer, to efficiently couple the damage in the microstructure with the strain field at the component level. Comparison is made with experimental observations of damage development in an axially-loaded composite tube, studied by X-ray computed tomography and digital volume correlation. Recommendations are made for futher development of the model to achieve greater fidelity to the microstructure.

Introduction

SiC-SiC$_{fibre}$ ceramic matrix composites are candidate materials for fuel cladding in Generation IV nuclear fission reactor concepts such as the gas cooled fast reactor (GFR) [1]. With excellent high temperature capability and damage tolerance, they may have future applications for accident-tolerant fuel cladding for current (Gen II/III) light water reactors (LWR) [2] and as structural materials in the tritium-breeding 'blanket' for nuclear fusion power generation [3]. SiC-SiC$_{fibre}$ composites have been developed largely within the international fusion materials' programmes, which have optimized their microstructures for thermo-mechanical properties in composites with unidirectional fibres or 2-dimensional weaves. Within the European nuclear fission programme, a tubular pin-type GFR fuel clad geometry with a filament wound and braided architecture has been designed [1] and layered monolithic SiC and SiC-SiC$_{fibre}$ composite structures have also been proposed for accident tolerant LWR fuel clad [4].

Component testing is critical for composites, in order to identify the potential role of the composite architecture and its defects. For these nuclear applications testing in realistic conditions of fast neutron flux and temperature will be essential eventually to evaluate fully these structures. Macroscopic mechanical tests (e.g. [5]) can be used to assess the average properties of the composite, and provide data for use in design. The effects of irradiation and oxidation, batch-batch variations in properties and also the sensitivity to composite fabrication can also be examined by such tests. Component tests will be critical also to evaluate the properties of complex structures of joints [6]. Stochastic property variations may occur due to heterogeneities in the weave [7], and this also needs to be quantified by testing. Test data are also needed for design, and a

*Author for correspondence (james.marrow@materials.ox.ac.uk).
†Department of Materials, University of Oxford, Parks Rd, Oxford, OX1 3PH, UK

possible structural design criterion for SiC-SiC$_{fibre}$ composites may be some fraction of the proportional limit stress (PLS)[8]. This is the critical stress, in tensile loading, above which non-linear stress/strain behaviour of the composite is observed. This non-linearity is caused by the development of significant matrix cracking [9], whilst the propagation of damage is resisted by the 'fibre pull out' toughening mechanism from the continuous, high strength SiC fibres [10,11]. Microcracking damage also affects the heat transfer properties of the cladding [12].

An understanding of failure mechanisms is needed to design of tests that will qualify materials for service, and also accelerated tests to understand the potential degradation of the mechanical properties of composites due to environmental factors. Predictive modelling of these materials in engineering components must be able to predict their performance under different states of loading, using data obtained in such tests. Continuum-mechanics methods can be insufficient for this, as they may not take into account the effects of the heterogeneous fabric architecture on the strain distribution that develops within the composite microstructure [13,14]. The strain distributions in woven fibre reinforced composites are influenced by factors that include the orientation of the fibre tow with respect to the loading axis [15], the arrangement and structure of neighbouring tows, matrix and pores [16], and also the mechanical properties of the composite's constituents [17,18]. Together, these may affect the statistical distribution of failure strength under different states of loading.

Numerical modelling is a staple ingredient of industrial component design and the assurance of structural integrity, particularly in civil, automobile, aerospace and nuclear engineering. These all need numerical methods that can deal with complex geometries and loading conditions, particularly to simulate the performance of real components under service loadings that cannot be reproduced experimentally. The need for sophisticated, efficient and reliable numerical models is demonstrated by their large expansion in the last decade, employing a wide range of approaches to advance their complexity and speed via alternative concepts and mathematical solutions that are frequently optimised to the problem under consideration. Probabilistic methods of structural integrity assessment require numerical tools to model damage, so numerical modelling is a necessary tool to simulate the behaviour of structural components that are made of ceramic composites [19].

All numerical computational models that have serious potential for engineering design employ discretization to break the problem into smaller units, e.g. the Finite Element (FE) method; their coupled behaviour describes the final result. In models that compute damage by fracture, and its interaction at the larger scale with the engineering structure, the discretization must be sufficiently fine to describe the critical micromechanical processes [20]. Damage may be introduced through a cohesive law to describe the microstructure properties, or via an explicit representation of the microstructure and its behaviour, so that that the energy released by damage within the microstructure is defined or calculated accurately [21,22]. Predicting the likelihood of failure and the patterns of damage propagation requires stochastic approaches, since the variability of microstructure can produce a range of larger scale responses [23] that depend on the size and geometry of the component. Consequently, the goal is to develop multiscale computational engineering models that have the necessary discretization to reproduce accurately the effects of microstructural damage [24] and yet have sufficient computational speed to simulate the stochastic behaviour of the component that will arise from microstructure heterogeneity[25].

One approach to computationally efficient multiscale modelling is to locally insert the microstructure into a coarser FE mesh, only where such refinement is needed (e.g. [19,26,27]). For instance, cohesive FE models may use a mesh that is adapted to key features of the microstructure such as the composite plies [28], with some models representing each tow of fibres explicitly [29]. The FEMME model for quasi-brittle materials [30]

uses the microstructure as a local enrichment of a coarse cohesive FE mesh. This approach has been applied to simulate damage development in a range of quasi-brittle materials including SiC-SiC composites [31] and thermal barrier coatings [32]. In this paper, it is applied to the problem of damage development in a ceramic fibre reinforced ceramic matrix composite tube. The objective is to demonstrate the ability of the FEMME model to introduce high fidelity to important aspects of the microstructure into a larger scale model of the component. This allows the sensitivity to microstructure heterogeneity to be explored. The characteristics that emerge from the model simulations can then be compared with experimental data that describe the bulk properties of the composite and the development of damage within its structure.

Experimental Observation of Damage Development by Tomography and Digital Volume Correlation

Damage development within a SiC-SiC ceramic composite tube has been studied recently by digital volume correlation (DVC) of laboratory X-ray computed tomographs. Brief details only are included here of an experiment that was conducted to examine damage development within a ceramic composite tube; full details are given in reference [33]. DVC is the three-dimensional analogue of digital image correlation (DIC), which is a displacement measurement method [34] that tracks the local movements within successive images that are due to deformation; it is well suited to the detection of damage [35] and has been applied previously to study deformation and damage in ceramic composites [9]. X-ray computed tomography (XCT) can be used to observe damage development *within* materials, including composites [31,36]. It can be combined with three-dimensional digital volume correlation [37] to measure the displacements that arise from deformation and damage [31,38,39].

The SiC-SiC material, provided by the MatISSe consortium [40], was fabricated by CEA (French Alternative Energies and Atomic Energy Commission), as described in ref. [9]; it comprised an inner SiC fibre filament wound layer (±45°) with two-layers of 2-dimensional braided structure (±45°). The inner and outer diameters were 7.80 and 9.75 mm respectively. A 55 mm length of the composite tube was tested in tension. Medium resolution computed tomography scans with a voxel size of 17 μm were obtained using a laboratory X-ray instrument. Higher resolution tomographs were used to characterise the porosity in the microstructure; an example image is shown in Figure 1. After a reference scan in the 'unloaded' state (at 20 N), the tube sample was mechanically loaded axially in tension; scans were obtained at loads of 400 N and 800 N, which correspond to axial tensile stresses of 17.3 MPa and 34.6 MPa. The sample was unloaded to 20 N and scanned by tomography between these loads. Digital volume correlation (DVC) analysis was applied to the tomographs, using the LaVision Davis software, to measure the three-dimensional full field displacements between successive tomographs. The reference tomograph was the initial unloaded specimen in each case. An anisotropic interrogation subset (128x128x256 voxels at 75% overlap, with the elongated dimension of the subset aligned parallel to the tube axis) was used.

The gradients of the measured displacement field can be used to obtain three-dimensional visualisations of the maximum principal strain, which are shown in Figure 2, for the tube under tensile load and after unloading. These illustrate the progressive development of localised strains that are distributed non-uniformly throughout the sample. The magnitudes of the strains decrease on unloading, but the pattern of strains remains. There is a greater degree of deformation towards the upper end of the tube, which is attributable to the method of sample mounting. The strains tend to occur on one side of the tube, indicating that there was some flexure introduced during the loading. These strains are due to damage in the microstructure, and arise from the opening displacements of cracks that tend to initiate from the significant porosity in the braided microstructure [33]. The DVC analysis is not sufficiently precise to measure elastic strains at this length-scale. The reported strains are due to the accumulated displacements from micro-cracking damage. An effective

strain of 0.01 is approximately equivalent to ~1 μm net displacement between adjacent displacement vectors, which have a separation of ~ 100 μm in the axial direction.

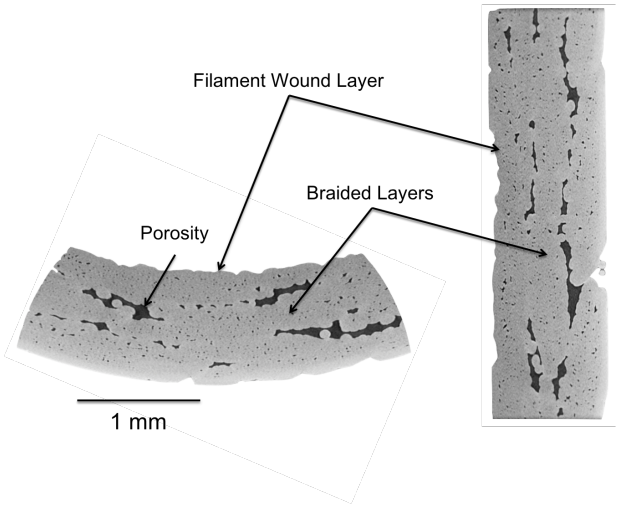

Figure 1: High resolution (1.7 μm voxel) computed X-ray tomographs of axial and longitudinal sections of a filament wound and braided SiC-SiC composite tube [33].

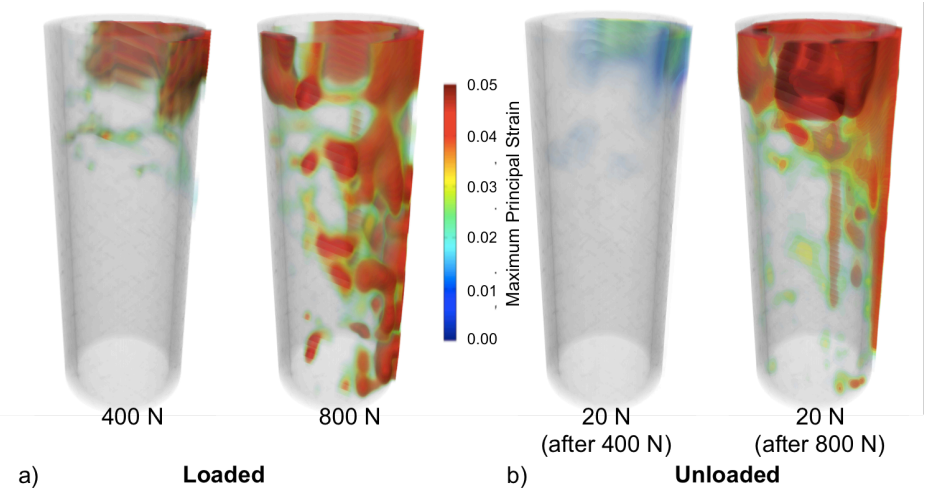

Figure 2: Visualisations of the maximum principal strain in a section of an axially loaded SiC-SiC composite tube, measured by digital volume correlation of computed X-ray tomographs: a) under load at 400 N and 800 N; b) unloaded to 20 N after being loaded to 400 N and 800 N. The tube diameter is approximately 10 mm [33].

Modelling of Damage Development

The FEMME Model for Damage Development in Quasibrittle Materials

The FEMME (Finite Element Microstructure MEshfree) model [30] is a multiscale model for fracture simulation that is designed to deal with the full scale of an engineering component and also the fine scale microstructural processes of damage efficiently. This is done through a combination of 3 layers that interact between each other and are located at different scales. The large scale is simulated through a standard finite element model (FEM) with a coarse mesh. If the strain of any element in the FEM reaches a critical strain, arbitrarily chosen and close to the critical strain of the material, the element is subdivided to create the cells and the other 2 layers are then activated locally. The first of these is a Microstructural Adaptive Meshfree layer (MAM), which is a meshfree model with exponential shape functions [41,42] that are geometrically adapted to the microstructural features, i.e. pores and particles that are defined as ellipsoids. The MAM model uses the nodal displacements of the subdivided elements of the FE mesh as its boundary conditions to calculate the displacements applied to the microstructural features. Those are interpolated into the third cellular layer to calculate the strain of each cell; these strains are evaluated against the cell's critical strain. If the strain of a cell is greater than its critical strain, the cell is damaged, releasing its elastic energy into fracture energy. The sum of the fracture energies of all the cells damaged at each iterative step of the simulation is used, through energy homogenization, to reduce the mechanical properties of the other layers. The effect is analogous to the cohesive laws employed in traditional FEM cohesive models; cohesive behaviour emerges from the operation of the CA layer. Depending on where each cell is located, it represents the matrix, the pores or the particles of the material, and its critical strain is assigned accordingly. With this, the heterogeneity of a microstructure is reproduced within a large scale FEM, without significant homogenisation of the microstructure.

One of the main potentialities of the FEMME model when compared with other fracture methodologies, is that it is able to release the spurious strain energy that is calculated using a coarse FE mesh during fracture simulation [30]. When a fracture process is modeled using a coarse FE mesh, the calculation of the fracture energy dissipated depends on the size of the mesh. This can lead to an overestimation of the peak load and a subsequent generation of spurious strain energy; this energy is not real and makes the FEM calculation completely invalid. The spurious fracture energy generated by a too-coarse mesh is a common drawback for the modeling of damage in large scale models, because it forces that FE mesh to be sufficiently fine to reduce this effect. The refined mesh increases exponentially the computational cost of the model and reducing its applicability. Through its multilayer approach, the FEMME model is able to release this spurious fracture energy by inserting locally the microstructure as a local enrichment that substitute for the mesh refinement traditional FE models require to solve this problem. Mesh refinements or predefinition of the fracture path are therefore not required. This decreases drastically the number of operations needed to solve the problem, compared to FEM at an equivalent level of discretisation. This is extremely beneficial to fracture problems where considerable numbers of iterations are needed to reach convergence at every loading step.

The model presented in the paper is an extension of the original FEMME model, and uses the same relationships between layers and method for the insertion of pores in the microstructure. The development here is the insertion of fibres, which influence both the FEM and MAM layers. An algorithm inserts the fibres using the mathematical description of each fibre tow to calculate how it crosses the element that it intersects. Mechanical properties are assigned to each fibre to describe the stress-strain behaviour and critical failure strain. A relationship between the strain of the element and the strain of the fibre is then established, so a reaction force from the fibre is obtained that can be applied at the nodes of the element that is crossed by the fibre as a boundary condition. This needs to be done iteratively, and in some cases relaxed to ensure the convergence and stability of the problem.

Extension of the FEMME model by Insertion of Fibres

This paper describes the extension of the FEMME model to consider damage in fibre-reinforced material with direct representation of the fibres. Previously, only the pores between fibre tows have been considered [31]. In this development, the fibres are inserted as a separate layer of the multiscale calculation, influencing both the FEM and MAM layers. Each fibre tow is first inserted in the FEM model as a single solid fibre; the individual fibres of the tow are then represented in the MAM model once the FE is subdivided and this region of the microstructure is activated. An alternative case would be where single fibres are not grouped in tows, such as in steel-fibre reinforced concrete, and here the same fibre could be inserted in both the FEM and MAM layers. The relationship between the FEM and MAM layers and the fibres is obtained through the strain field of those models and the equivalent load that is inserted from the fibres as a reaction force. For this each finite element that is crossed by a fibre tow has associated with it a simplified straight fibre tow segment that connects the crossing points where the fibre tow enters and leaves the element (Figure 3a).

To calculate the positions of these crossing points, each fibre tow is defined through the parametric mathematical expression of the locus of its central axis. Then, the problem is reduced to the calculation of the crossing point between the plane formed by each side of the tetrahedral element and the mathematical expression of the fibre tow. The crossing points between the parametric description of the fibre tow and the FE is shown in Figure 3a, with the simplified straight fibre that represents the fibre tow within the element. In Figure 3b the relationship between the fibres and the microstructure is presented, with the region where the fibres are inserted in the mechanical model of the MAM layer; this shows the inter-particle domains that are defined between pores. All the crossing points are evaluated and the pairs that lies at the borders of the tetrahedron is selected to define the fibre path [43]. The same algorithm is also used with the tetrahedrons that define the inter-particle domains of the MAM layer [30].

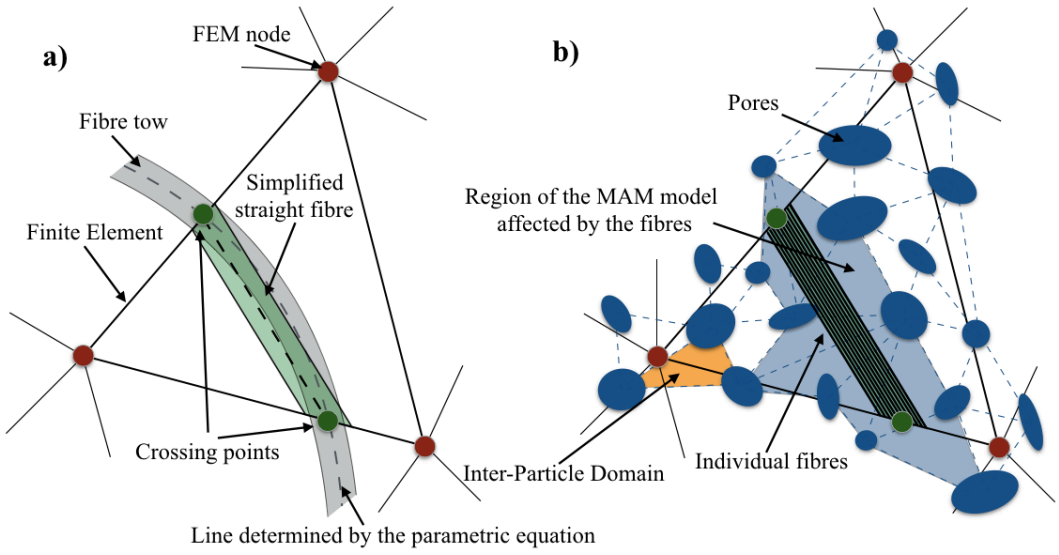

Figure 3: Relationship between a Finite Element, the microstructure, a fibre tow and its fibres: a) in the FEM (finite element model) layer, and b) the MAM (Microstructural Adaptive Meshfree) layer.

Any fibre typology can be implemented using its mathematical description. In the case of the SiC-SiC fibre composite that is considered in this paper, the fibres can be approximately described by equations 1 to 4. As noted, this composite comprises an inner SiC fibre filament wound layer (±45°) with two-layers of 2-dimensional braided structure (±45°). There are flat pores located in the intersections between the fibre tows and longitudinal pores (long and short) located along the fibre direction [33] (Figure 1). The braiding effect is implemented through a combination of sine and cosine curves, with the parameter u that grows in the Cartesian x direction (Figure 4a). With these equations each fibre tow of the 3 superimposed braided layers can be characterized:

$$x = f(u) = u \pm c \qquad (1)$$

$$R_{loc} = R_{tube} \pm \Delta R \cdot \cos\left(\frac{\pi \cdot x}{d}\right) \qquad (2)$$

$$y = g(u) = \pm R_{loc} \cdot \sin(A \cdot u) \qquad (3)$$

$$z = h(u) = \left(\frac{|\cos(A \cdot u)|}{\cos(A \cdot u)}\right) \cdot \sqrt{R_{loc}^2 \cdot (1 - \sin^2(A \cdot u))} \qquad (4)$$

In equations 1 to 4, x, y and z are the Cartesian coordinates of the parametric plot. The parameter c is used to create different parallel fibres or fibre tows starting in different points. R_{tube} is the average radius of the layer; ΔR is the maximum variation of this radius given by the braiding, where d controls the amplitude of the braiding. A is the amplitude of the main fibre bundle (i.e. each tow describes an spiral, so A is the distance between peaks of a complete loop). The plus and minus signs are for the two sets of fibre directions, depending in which direction the spirals are growing (Figure 4b).

These equations describe the position of the central axis of each fibre tow, and then the cross-section area needs to be inserted as a surface orthogonal to the tow axis. For the micromechanical model, the crossings of each individual fibre and the tetrahedrons of the MAM layer are computed after the Finite Element that hosts this part of the microstructure is subdivided into domains. Each individual fibre is considered as a straight segment that is parallel to the path formed by the two crossing points of the Finite Element that is associated with the fibre tow. As the fibre tows are not fully dense, the individual fibres are positioned randomly within the associated cross-section area of the fibre tow that is inserted in the FE model (see Figure 3c). The individual fibres are not continuous across the elements, and do not overlap. They are inserted randomly until the sum cross sectional area of the fibres is equal to a pre-determined proportion (80%) of the cross section of the fibre tow. The remainder of the cross-section represents the matrix and pores that are within the fibre tow. Once all the crossings between the fibres and tetrahedrons are computed, this information is used for the mechanical model. In each tetrahedron of the FE and MAM layers that is crossed by a fibre or fibre tow, there is a segment that is defined by the 2 crossing points and has a description of its orientation, solid area and mechanical properties.

The interaction between the fibre and the tetrahedron needs to reproduce the real behaviour of the material. Firstly the strain state of the fibre needs to be determined by considering its stress-strain relationship. Assuming a perfect bond between the fibre tow and the matrix, the strain state of the tetrahedron in the FE layer is projected into the fibre direction to determine the effective strain along the fibre. In future developments of the model, through the damage of the CA layer, the state of the bond can be evaluated and the adherence of the fibre will be reproduced, increasing the accuracy of the model. Presently, this is addressed by tuning the non-linear stress-strain behaviour of each fibre to produce a stress-strain function that represents the mechanical response at the length scale of the cellular description of the microstructure due to

matrix damage and fibre-pull out. Once the strain of the fibre is determined, through its stress-strain behaviour and the area of the fibre, the reaction force applied by the fibre into the tetrahedron is determined. This force is shared between the nodes of the tetrahedron with an opposite sign, i.e. if a tensile strain is applied to the fibre, the forces to be applied in the nodes will make compression. With this the influence of the fibres on the matrix is reproduced. Then those forces are inserted in the FE model as Neumann (or second type) boundary conditions. These need to be relaxed iteratively. For a material with a low content of fibres (i.e. reinforced concrete) the problem is relaxed by simply applying the strains of the fibres in the FE model, which should be run until the convergence of the strains in the fibres. For the case where the material is mainly composed by fibres (e.g. SiC-SiC fibre composites), the convergence is not reached through the direct iteration of the model, and the fibre forces need to be inserted gradually in different iterations to ensure the gradual convergence of the material. This is feasible due to the computational efficiency of the FEMME model.

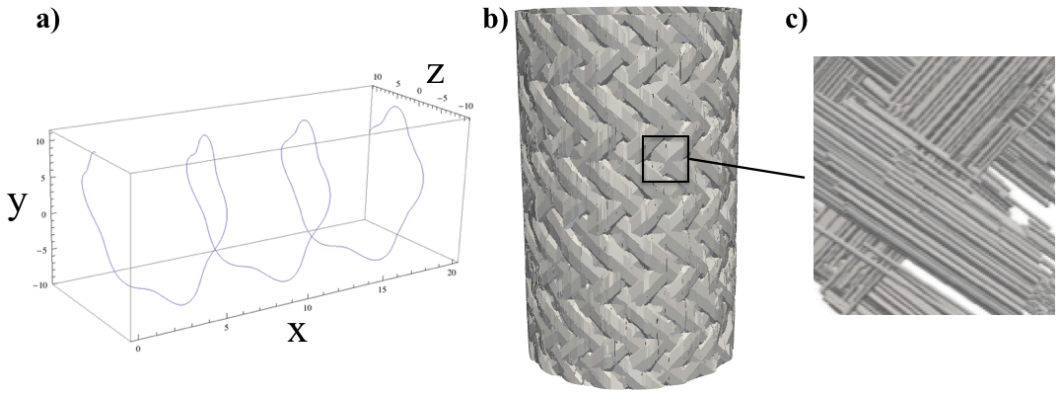

Figure 4: Description of the fibres at different levels; a) the parametric equation of a fibre tow, b) the pattern of fibre tows in the tube and c) a zoomed subdivision of the fibre tows into its fibres.

Simulation of a SiC-SiC fibre Composite under Tensile Axial Load

In this example we use the model to simulate an experiment in which a tube with the SiC-SiC fibre composite described is loaded in tension. In the experiment described above, distributed damage was observed within the composite. The detailed study of Bernachy-Barbe et al [9] measured the bulk properties of the same material, and studied damage development using digital image correlation of the external tube surface together with acoustic emission. Together, these provide some observations against which the model simulations may be compared.

The geometry of the tube was reproduced by the FE layer, and the microstructure of the material was described in the MAM and CA layers. The FE mesh that describes the composite tube is composed of only 3228 tetrahedral elements, with an element size of 1.5 mm (Figure 5). The total tube length is 68 mm and all the applied displacements are null except the axial displacement (i.e. x direction) of the top of the tube that is applied uniformly to represent the experiment loading. The internal diameter is 8 mm and the external is 10 mm. The 3 superimposed braided layers occupy the wall thickness of 1 mm. Each Finite Element may be subdivided into 4096 cells to simulate its damage, so the discretization size (i.e. cell size) is 50 μm. This is larger than the 12 μm diameter of the fibres, so their representation is an approximation.

The microstructure is inserted to represent the porosity of the matrix and the fibres. To create the different types of pores we consider their size as ellipsoids and their orientation [43]. Pores between fibre tows that are located where tows cross each other, are defined by their centre, and are aligned tangentially to the fibre tow layer. The longitudinal pores are also ellipsoidal, and are aligned with the fibre direction. Both pore shapes are introduced using the equations 1-4 to locate the position of its centre and orientation with respect to the fibre tows, and the shape of the tube to align them orthogonal to the tube radius. The total porosity measured by experiment (~5%) [33] is reproduced in the model; By volume, 35% are flat pores and 65% are longitudinal, and by number 6% are flat pores and 94% are longitudinal. A comparison between the numerical and experimental microstructures is shown in Figure 6. The cross-section of the numerical pores (Figure 6b) agrees with the segmented tomograph of the real material where the thin pores are distributed across the thickness and the flat pores are between the braided layers. Visualizations of the numerical fibres and the material surface are shown in Figure 6c. With this, the computational time of the model is 8 hours running in serial in a Pentium i7 processor.

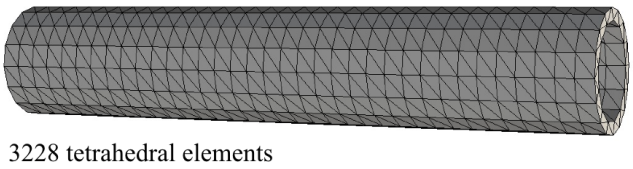

Figure 5: FE mesh used for the model of the tube with 68 mm long, 5 mm external radius and 1 mm wall thickness.

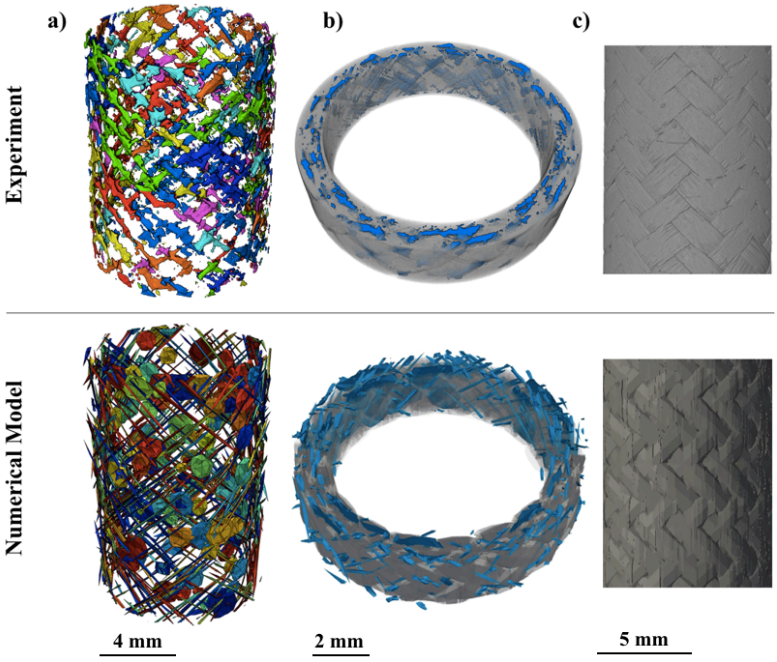

Figure 6: Comparison between the numerical and experimental microstructure characterized through a tomograph [33]. a) shows the large porosity, b) a orthogonal cut of the porosity and c) the fibres tows.. Different pores are identified by colour.

Having developed a model description of the microstructure, the aim is to fit the simulation to the experimental results of Bernachy-Barbe et al [9], and to examine the predicted development of damage. In that experiment, the authors applied a tensile load to a SiC-SiC composite tube of 68 mm length, with careful observation by extensometry of the axial and radial strains of the tube. In the FEMME simulation, the mechanical properties used are: for the fibres, a Young modulus of 400 GPa, an elastic strain limit of 0.0125% and a failure strain of 2%, with linear strain softening from the elastic limit; for the matrix, the Young Modulus is 100 GPa, the critical elastic failure strain 0.025% and Poisson's ratio is 0.26. Those material properties are an optimised fit that reproduces the bulk behaviour of the material (Figure 7).

The predicted development of damage for these properties is shown in Figure 8, which presents the maximum principal strains within the tube at different applied axial strains (see Figure 7a). Damage initiates from a significant pore from an early stage (from a tensile stress of approximately 70 MPa) with non-linearity apparent above approximately 110 MPa. As the applied strain is increased, the damage propagates through the central region and causes gradual failure of fibre tows. The stress field around the damaged region is shown in Figure 8b.

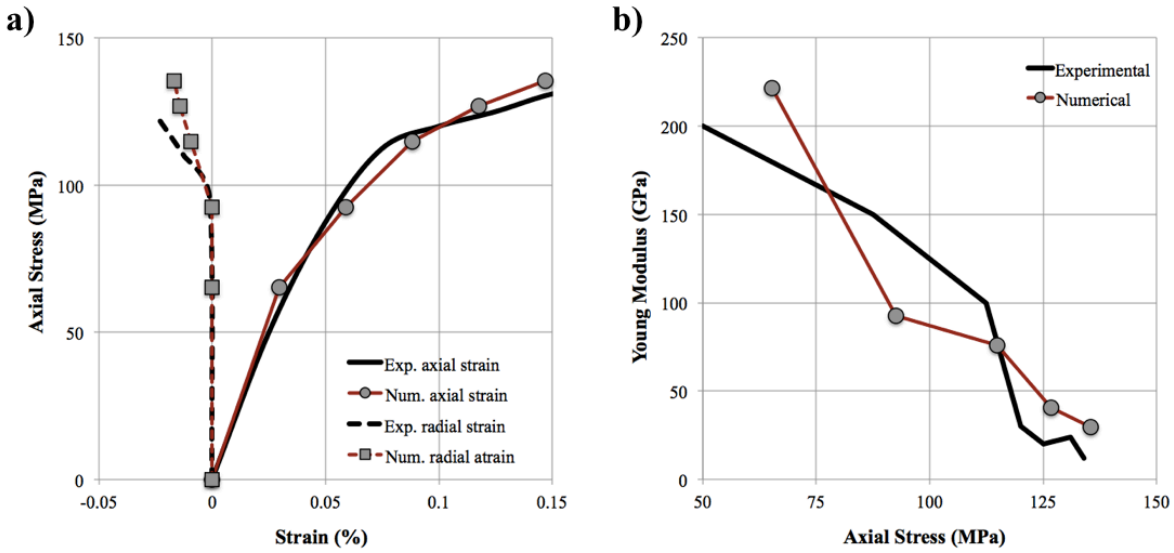

Figure 7: Comparison between the numerical results and the experimental data [9] of the a) stress-strain behaviour and b) the decay of the tensile Young modulus with applied bulk stress.

Simulation of a SiC-SiC fibre composite under Internal Pressure

Having demonstrated the capabilities of the model to reproduce the bulk behaviour of the material in one stress state, it may be applied to examine the expected performance under different stress states, such as internal pressure. In this case the microstructure of the simulated sample is the same that was used in the example of tensile loading. The predicted nucleation and growth of damage in the deformed tube (without magnification of displacements) is shown in Figure 9, as pressure is increased progressively to 150 MPa. The simulation is an approximation, as the applied internal pressure is not relieved by damage to the tube. Damage first appears at 50 MPa internal pressure, i.e. at a hoop stress of approximately 200 MPa and axial

stress 100 MPa. The developed damage is aligned longitudinally, due to the hoop stress, but the critical damage nucleates at a different location to the tensile loaded case.

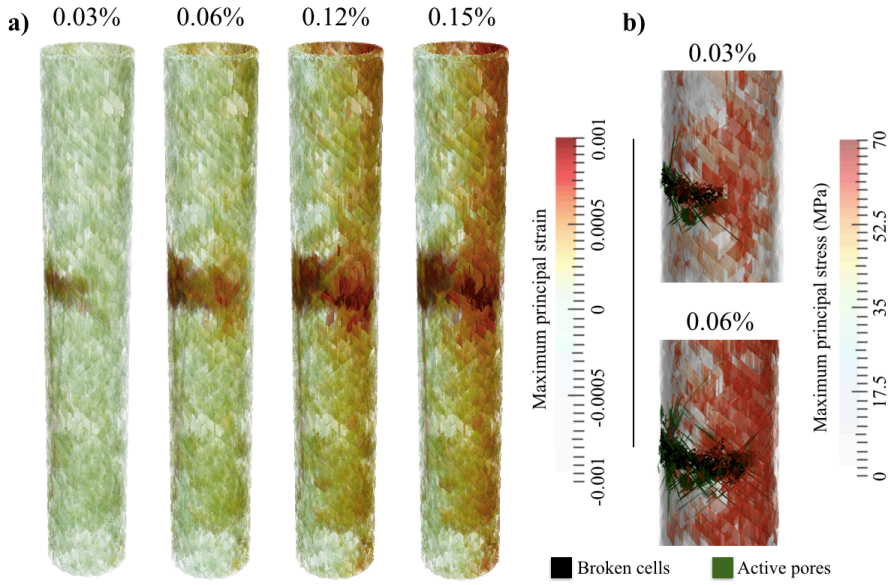

Figure 8: Simulation of damage in the SiC-SiC composite tube; a) Strains of the tube at different bulk deformations, and b) stress state of a zoomed region around the crack tip at different bulk deformations.

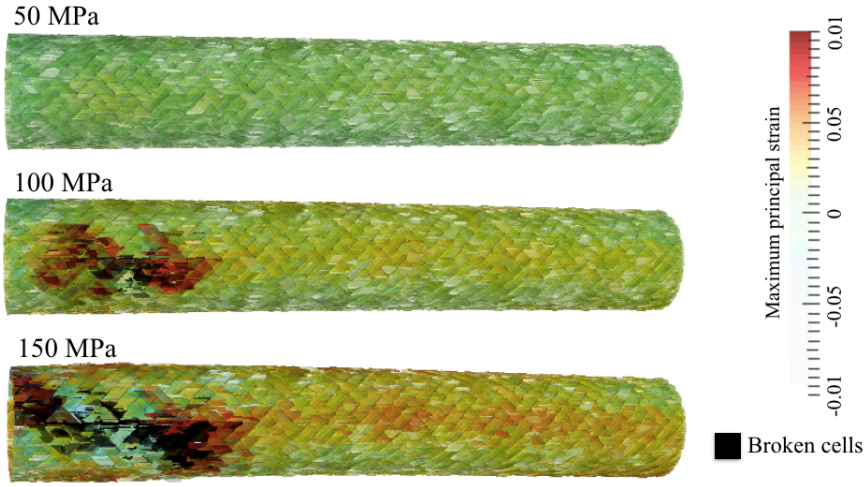

Figure 9: Simulation of the development of strain and damage in the SiC-SiC composite tube under an increasing internal pressure.

Simulation of Variability in Fibre Tow Properties

The described model framework is suited to examine the influence of defects in the material, and also of variability of the properties of the fibres and matrix since the material properties are taken from statistical distributions of the strength of every phase and the geometry of microstructure is described in detail. Due to the low computational cost of the model, it may be used to perform a sensitivity analysis to identify the key material factors. As an example, Figure 10 shows the same model of tensile loading (i.e. Figure 8) in which the effects of random defects that affect the fibres tows have been studied. This is done: i) by decreasing the elastic limit stress of 20% of a random selection of the fibre segments by 10 MPa (i.e. by 20%); and ii) by additionally reducing in the same segments the fibre failure strain to 0.02%. The effect of this on the bulk behaviour of the composite tube is quite apparent; the weakening of the fibre tows leads to more distributed damage and earlier softening of the composite as the applied strain increases.

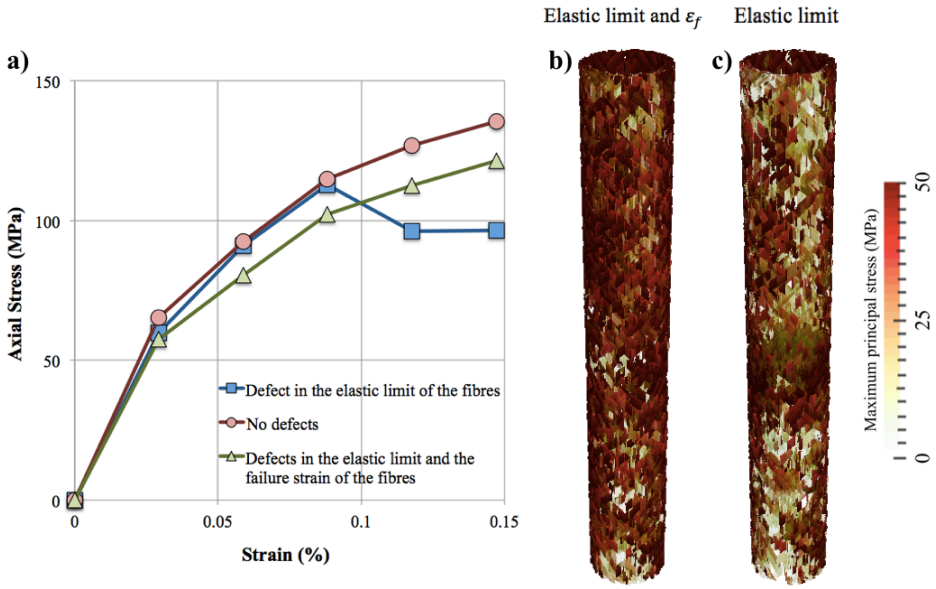

Figure 10: a) axial stress-strain behaviour of the tube with the same microstructure and fibre pattern, but with defects randomly distributed within the volume and represented by reductions in the elastic limit and failure strain of the fibres; b) and c) show the stress of the fibres for the 2 different defect types.

Discussion

The aim of the presented model is to address the gap between the modelling of the full-scale component and micromechanical damage, by introducing the influence of the fibres. The fibres inserted in the FEMME model have the potential to arrest a crack that is propagating, increase the stiffness of the component and increase the load that is transferred across the crack faces. The model therefore approximates the influence of the fibres on composite behaviour.

In its current form, the FEMME model allows the effects of the significant pores between fibre tows to be simulated, and the effects of stress state on damage development and propagation in the composite component to be examined. The predicted patterns of damage are consistent with experimental observations (i.e. Figure 2 and Figure 8. The stresses that develop damage in the tube under tensile and pressure loading are also described; the critical stresses that cause damage with internal pressure are comparable to those measured experimentally [9]. The change in the location of the onset of significant damage between tensole and pressure loading demonstrates the importance of the geometry and location of defects relative to the local stresses in the composite microstructure. The simulation of material variability (Figure 10) also shows that variations in the ability to sustain load by fibre-pull out may have a significant effect on the bulk properties of the composite.

In an experimental study [44] of the tensile behaviour of single tows of aligned SiC fibres with a SiC matrix, the Young modulus of a single fibre tow was reported as 375 GPa and the elastic limit approximately 500 MPa. Matrix cracking around the fibre tow occurred above 0.1% strain (i.e. close to the elastic limit), with ultimate failure at around 0.7% strain. Compared to this, the properties applied in the FEMME simulation that give good agreement with the experimental properties of the composite tube appear quite low. This is because the simulation is designed to address the effects of the significant stress concentrating pores and defects at the interfaces of the fibre tows. The simulation does not directly reproduce the pull out of the fibres, and the input properties describe the influence of strain on the load that is carried by the fibres that are represented within the component. The elastic limit for the fibre tows in the FEMME model is thus the strain (0.0125%) at which interface damage is assumed to begin at the fibre tow, and the failure strain represents the fibre pull out limit when it cannot carry load. Higher resolution modelling that is more fundamentally related to the structure of the fibre tows and their interfaces would be needed to directly relate the FEMME model input properties to the physical properties of the composite constituents.

Future extensions of this model will allow one to address the development of damage of the composite at high temperature, which will influence its thermal properties [32] and simulate the effects of fast neutron irradiation and oxidation on composite performance due to changes in local properties. The FEMME model may also be, inserted into other numerical frameworks for modelling of fibrous structures (e.g. [45]), which would provide more representative descriptions of composite weaves and their defects [46], and also of non-uniformity of their deformation under shear loading, for example.

Conclusions

A numerical modelling framework has been applied (FEMME) which aims to capture the key features of the ceramic composite microstructure that control damage development, particularly the location, orientation and geometry of significant porosity and the load-carrying capability and quasi-brittle failure behaviour of the ceramic fibre tows. This allows a high fidelity numerical simulation to be performed that describes damage development at a length scale that can be studied experimentally. The simulations performed can describe the failure of the component under different states of stress and can obtain good agreement with bulk properties. Sensitivity to the potential degradation of material properties is also obtained. The general characteristics of the predicted damage are also consistent with experimental observations. The model requires further development to achieve high fidelity to microstructural processes such as matrix cracking and fibre pull-out.

Additional Information

Funding Statement

L. Saucedo-Mora was funded by the UK EPSRC project "QUBE: Quasi-Brittle fracture: a 3D Experimentally-validated approach" (EP/J019992/1, principal investigator T.J. Marrow). TJ Marrow acknowledges the support of the Oxford Martin School. This work also contributes to Work Package 3 of the MatISSe Collaborative Project "Materials' Innovations for Safe and Sustainable Nuclear" (European Commission Seventh Framework Programme Grant 604862, FP7-Fission-2013).

Competing Interests

The authors have no competing interests.

Authors' Contributions

L. Saucedo-Mora conducted the modelling simulations that are described in this paper, under the academic supervision of TJ Marrow. Both authors jointly conceived the analysis, interpreted the data and wrote the paper.

References

1. Carre, F., Yvon, P., Anzieu, P., Chauvin, N. & Malo, J.-Y. 2010 Update of the French R&D strategy on gas-cooled reactors. *Nucl. Eng. Des.* **240**, 2401–2408. (doi:10.1016/j.nucengdes.2010.02.042)

2. Sauder, C., Michaux, A., Loupias, G., Billaud, P. & Braun, J. 2013 Assessment of SiC/SiC cladding for LWRs. In *LWR Fuel Performance Meeting, Top Fuel 2013*, pp. 951–956. American Nuclear Society.

3. Katoh, Y., Snead, L. L., Henager, C. H., Hasegawa, A., Kohyama, A., Riccardi, B. & Hegeman, H. 2007 Current status and critical issues for development of SiC composites for fusion applications. *J. Nucl. Mater.* **367-370**, 659–671. (doi:10.1016/j.jnucmat.2007.03.032)

4. Deck, C. P., Jacobsen, G. M., Sheeder, J., Gutierrez, O., Zhang, J., Stone, J., Khalifa, H. E. & Back, C. A. 2015 Characterization of SiC–SiC composites for accident tolerant fuel cladding. *J. Nucl. Mater.* **466**, 667–681. (doi:10.1016/j.jnucmat.2015.08.020)

5. Jacobsen, G. M., Stone, J. D., Khalifa, H. E., Deck, C. P. & Back, C. A. 2014 Investigation of the C-ring test for measuring hoop tensile strength of nuclear grade ceramic composites. *J. Nucl. Mater.* **452**, 125–132. (doi:10.1016/j.jnucmat.2014.05.002)

6. Ferraris, M., Salvo, M. & Casalegno, V. 2011 *Ceramic Integration and Joining Technologies*. Hoboken, NJ, USA: John Wiley & Sons, Inc. [cited 2016 Feb. 8]. (doi:10.1002/9781118056776)

7. Nozawa, T., Lara-Curzio, E., Katoh, Y. & Shinavski, R. J. 2008 Tensile properties of advanced

SiC/SiC composites for nuclear control rod applications. In *Ceramic Engineering and Science Proceedings*, pp. 223–234.

8. Nozawa, T., Kim, S., Ozawa, K. & Tanigawa, H. 2014 Stress envelope of silicon carbide composites at elevated temperatures. *Fusion Eng. Des.* (doi:10.1016/j.fusengdes.2013.12.032)

9. Bernachy-Barbe, F., Gélébart, L., Bornert, M., Crépin, J. & Sauder, C. 2015 Anisotropic damage behavior of SiC/SiC composite tubes: Multiaxial testing and damage characterization. *Compos. Part A Appl. Sci. Manuf.* **76**, 281–288. (doi:10.1016/j.compositesa.2015.04.022)

10. Lissart, N. & Lamon, J. 1997 Damage and failure in ceramic matrix minicomposites: Experimental study and model. *Acta Mater.* **45**, 1025–1044.

11. Lamon, J. 2014 *Ceramic Matrix Composites*. Hoboken, NJ, USA: John Wiley & Sons, Inc. [cited 2016 Feb. 8]. (doi:10.1002/9781118832998)

12. El Yagoubi, J., Lamon, J., Batsale, J.-C., Dhote, J. & Le Flem, M. 2015 Multiscale Thermal Characterization of Mechanically Loaded Ceramic Matrix Composite. *Exp. Mech.* **55**, 783–794. (doi:10.1007/s11340-014-9976-x)

13. Shaw, J. H., Rossol, M. N., Marshall, D. B. & Zok, F. W. 2015 Effects of Tow-Scale Holes on the Mechanical Performance of a 3D Woven C/SiC Composite. *J. Am. Ceram. Soc.* **98**, 948–956. (doi:10.1111/jace.13389)

14. Mahadik, Y., Brown, K. A. R. & Hallett, S. R. 2010 Characterisation of 3D woven composite internal architecture and effect of compaction. *Compos. Part A Appl. Sci. Manuf.* **41**, 872–880. (doi:10.1016/j.compositesa.2010.02.019)

15. Komeili, M. & Milani, A. S. 2012 The effect of meso-level uncertainties on the mechanical response of woven fabric composites under axial loading. *Comput. Struct.* **90-91**, 163–171. (doi:10.1016/j.compstruc.2011.09.001)

16. Vanaerschot, A., Cox, B. N., Lomov, S. V. & Vandepitte, D. 2013 Stochastic multi-scale modelling of textile composites based on internal geometry variability. *Comput. Struct.* **122**, 55–64. (doi:10.1016/j.compstruc.2012.10.026)

17. Krenkel, W. 2008 *Ceramic Matrix Composites*. Weinheim, Germany: Wiley-VCH Verlag GmbH & Co. KGaA. [cited 2016 Feb. 17]. (doi:10.1002/9783527622412)

18. Fagiano, C., Genet, M., Baranger, E. & Ladevèze, P. 2014 Computational geometrical and mechanical modeling of woven ceramic composites at the mesoscale. *Compos. Struct.* **112**, 146–156. (doi:10.1016/j.compstruct.2014.01.045)

19. Yang, Q. & Naderi, M. 2015 *Numerical Modelling of Failure in Advanced Composite Materials*. Elsevier. [cited 2016 Feb. 5]. (doi:10.1016/B978-0-08-100332-9.00010-4)

20. Nalla, R. K., Kinney, J. H. & Ritchie, R. O. 2003 Mechanistic fracture criteria for the failure of human cortical bone. *Nat. Mater.* **2**, 164–8. (doi:10.1038/nmat832)

21. Carpinteri, A. & Colombo, G. 1989 Numerical analysis of catastrophic softening behaviour (snap-back instability). *Comput. Struct.* **31**, 607–636. (doi:10.1016/0045-7949(89)90337-4)

22. Moës, N. & Belytschko, T. 2002 Extended finite element method for cohesive crack growth. *Eng. Fract. Mech.* **69**, 813–833. (doi:10.1016/S0013-7944(01)00128-X)

23. Bazant, P, Z. 2001 Probabilistic modeling of quasibrittle fracture and size effect. In *Structural safety and Reliability* (ed Corotis et al. (eds)), pp. 1–23. Swets & Zeitinger.

24. Belytschko, T. & de Borst, R. 2010 Multiscale Methods in Computational Mechanics. *Int. J. Numer. Methods Eng.* **83**, 939–939. (doi:10.1002/nme.3013)

25. Arregui-Mena, J. D., Margetts, L. & Mummery, P. M. 2014 Practical Application of the Stochastic Finite Element Method. *Arch. Comput. Methods Eng.* (doi:10.1007/s11831-014-9139-3)

26. Ismar, H. & Streicher, F. 1999 Modelling and simulation of the mechanical behavior of ceramic matrix composites as shown by the example of SiC/SiC. *Comput. Mater. Sci.* **16**, 17–24. (doi:10.1016/S0927-0256(99)00041-5)

27. El Said, B., Ivanov, D., Long, A. C. & Hallett, S. R. 2014 Multi-scale modeling of 3D woven structures for mechanical performance. In *16th European Conference on Composite Materials, ECCM 2014*, European Conference on Composite Materials, ECCM.

28. Kumar, R. S. 2013 Analysis of coupled ply damage and delamination failure processes in ceramic matrix composites. *Acta Mater.* **61**, 3535–3548. (doi:10.1016/j.actamat.2013.02.027)

29. Grujicic, M., Snipes, J. S., Galgalikar, R., Yavari, R., Avuthu, V. & Ramaswami, S. 2015 Multi-length-scale derivation of the room-temperature material constitutive model for SiC/SiC ceramic-matrix composites. *Proc. Inst. Mech. Eng. Part L J. Mater. Des. Appl.* (doi:10.1177/1464420715600002)

30. Saucedo-Mora, L. & Marrow, T. J. 2015 FEMME: A multi-scale Finite Element Microstructure MEshfree fracture model for quasi-brittle materials with complex microstructures. *Eng. Fract. Mech.* **147**, 355–372. (doi:10.1016/j.engfracmech.2015.05.059)

31. Saucedo-Mora, L., Mostafavi, M., Khoshkhou, D., Reinhard, C., Atwood, R., Zhao, S., Connolly, B. & Marrow, T. J. 2016 Observation and simulation of indentation damage in a SiC–SiCfibre ceramic matrix composite. *Finite Elem. Anal. Des.* **110**, 11–19. (doi:10.1016/j.finel.2015.11.003)

32. Saucedo-Mora, L., Slámečka, K., Thandavamoorthy, U. & Marrow, T. J. 2015 Multi-scale modeling of damage development in a thermal barrier coating. *Surf. Coatings Technol.* **276**, 399–407. (doi:10.1016/j.surfcoat.2015.06.038)

33. Saucedo-Mora, L., Lowe, T., Lee, P. D., Mummery, P. M. & Marrow, T. J. In press. In situ observation of mechanical damage within a SiC-SiC ceramic matrix composite.

34. Hild, F. & Roux, S. 2006 Digital Image Correlation: from Displacement Measurement to Identification of Elastic Properties - a Review. *Strain* **42**, 69–80. (doi:10.1111/j.1475-1305.2006.00258.x)

35. Mostafavi, M. & Marrow, T. J. 2012 Quantitative in situ study of short crack propagation in polygranular graphite by digital image correlation. *Fatigue Fract. Eng. Mater. Struct.* **35**, 695–707. (doi:10.1111/j.1460-2695.2012.01648.x)

36. Chateau, C., Gélébart, L., Bornert, M., Crépin, J., Boller, E., Sauder, C. & Ludwig, W. 2011 In situ X-ray microtomography characterization of damage in SiCf/SiC minicomposites. *Compos. Sci. Technol.* **71**, 916–924. (doi:10.1016/j.compscitech.2011.02.008)

37. Bay, B. K., Smith, T. S., Fyhrie, D. P. & Saad, M. 1999 Digital volume correlation: Three-dimensional strain mapping using x-ray tomography. *Exp. Mech.* **39**, 217–226.

38. Mostafavi, M. et al. 2015 Yield behavior beneath hardness indentations in ductile metals, measured by three-dimensional computed X-ray tomography and digital volume correlation. *Acta Mater.* **82**, 468–482. (doi:10.1016/j.actamat.2014.08.046)

39. Vertyagina, Y., Mostafavi, M., Reinhard, C., Atwood, R. & Marrow, T. J. 2014 In situ quantitative three-dimensional characterisation of sub-indentation cracking in polycrystalline alumina. *J. Eur. Ceram. Soc.* **34**, 3127–3232. (doi:10.1016/j.jeurceramsoc.2014.04.002)

40. Cabet, C., Michaux, A., Fazio, C., Malerba, L., Maday, M. F., Serrano, M. & Nilsson, K. F. 2013 The new EC FP7 MatISSE project: materials' innovations for a safe and sustainable nuclear in Europe. In *SMINS-3, Structural Materials for Innovative Nuclear Systems (SMINS-3) - Workshop Proceedings, Idaho National Laboratory, Idaho Falls, United States, 7-10 October 2013*, [cited 2016 Feb. 8].

41. Arroyo, M. & Ortiz, M. 2006 Localmaximum-entropy approximation schemes: a seamless bridge between finite elements and meshfree methods. *Int. J. Numer. Methods Eng.* **65**, 2167–2202. (doi:10.1002/nme.1534)

42. Saucedo Mora, L. 2012 Meshfree methods applied to tensile fracture and compressive damage in quasi-brittle materials.

43. Saucedo-Mora, L. & Marrow, T. J. 2015 Method for the explicit insertion of microstructure in Cellular Automata Finite Element (CAFE) models based on an irregular tetrahedral Finite Element mesh: Application in a multi-scale Finite Element Microstructure MEshfree framework (FEMME). *Finite Elem. Anal. Des.* **105**, 56–62. (doi:10.1016/j.finel.2015.07.001)

44. Sauder, C., Brusson, A. & Lamon, J. 2010 Influence of Interface Characteristics on the Mechanical Properties of Hi-Nicalon type-S or Tyranno-SA3 Fiber-Reinforced SiC/SiC Minicomposites. *Int. J. Appl. Ceram. Technol.* **7**, 291–303. (doi:10.1111/j.1744-7402.2010.02485.x)

45. Green, S. D., Long, A. C., El Said, B. S. F. & Hallett, S. R. 2014 Numerical modelling of 3D woven preform deformations. *Compos. Struct.* **108**, 747–756. (doi:10.1016/j.compstruct.2013.10.015)

46. Melenka, G. W., Lepp, E., Cheung, B. K. O. & Carey, J. P. 2015 Micro-computed tomography analysis of tubular braided composites. *Compos. Struct.* **131**, 384–396. (doi:10.1016/j.compstruct.2015.05.057)

Figure and table captions

Figure 1: High resolution (1.7 μm voxel) computed X-ray tomographs of axial and longitudinal sections of a filament wound and braided SiC-SiC composite tube [33].

Figure 2: Visualisations of the maximum principal strain in a section of an axially loaded SiC-SiC composite tube, measured by digital volume correlation of computed X-ray tomographs: a) under load at 400 N and 800 N; b) unloaded to 20 N after being loaded to 400 N and 800 N. The tube diameter is approximately 10 mm [33].

Figure 3: Relationship between a Finite Element, the microstructure, a fibre tow and its fibres: a) in the FEM (finite element model) layer, and b) the MAM (Microstructural Adaptive Meshfree) layer.

Figure 4: Description of the fibres at different levels; a) the parametric equation of a fibre tow, b) the pattern of fibre tows in the tube and c) a zoomed subdivision of the fibre tows into its fibres.

Figure 5: FE mesh used for the model of the tube with 68 mm long, 5 mm external radius and 1 mm wall thickness.

Figure 6: Comparison between the numerical and experimental microstructure characterized through a tomograph [33]. a) shows the large porosity, b) a orthogonal cut of the porosity and c) the fibres tows.. Different pores are identified by colour.

Figure 7: Comparison between the numerical results and the experimental data [9] of the a) stress-strain behaviour and b) the decay of the tensile Young modulus with applied bulk stress.

Figure 8: Simulation of damage in the SiC-SiC composite tube; a) Strains of the tube at different bulk deformations, and b) stress state of a zoomed region around the crack tip at different bulk deformations.

Figure 9: Simulation of the development of strain and damage in the SiC-SiC composite tube under an increasing internal pressure.

Figure 10: a) axial stress-strain behaviour of the tube with the same microstructure and fibre pattern, but with defects randomly distributed within the volume and represented by reductions in the elastic limit and failure strain of the fibres; b) and c) show the stress of the fibres for the 2 different defect types.